Volume 24
Number 47
21 December 2022
Pages 8189–8340

CrystEngComm

rsc.li/crystengcomm

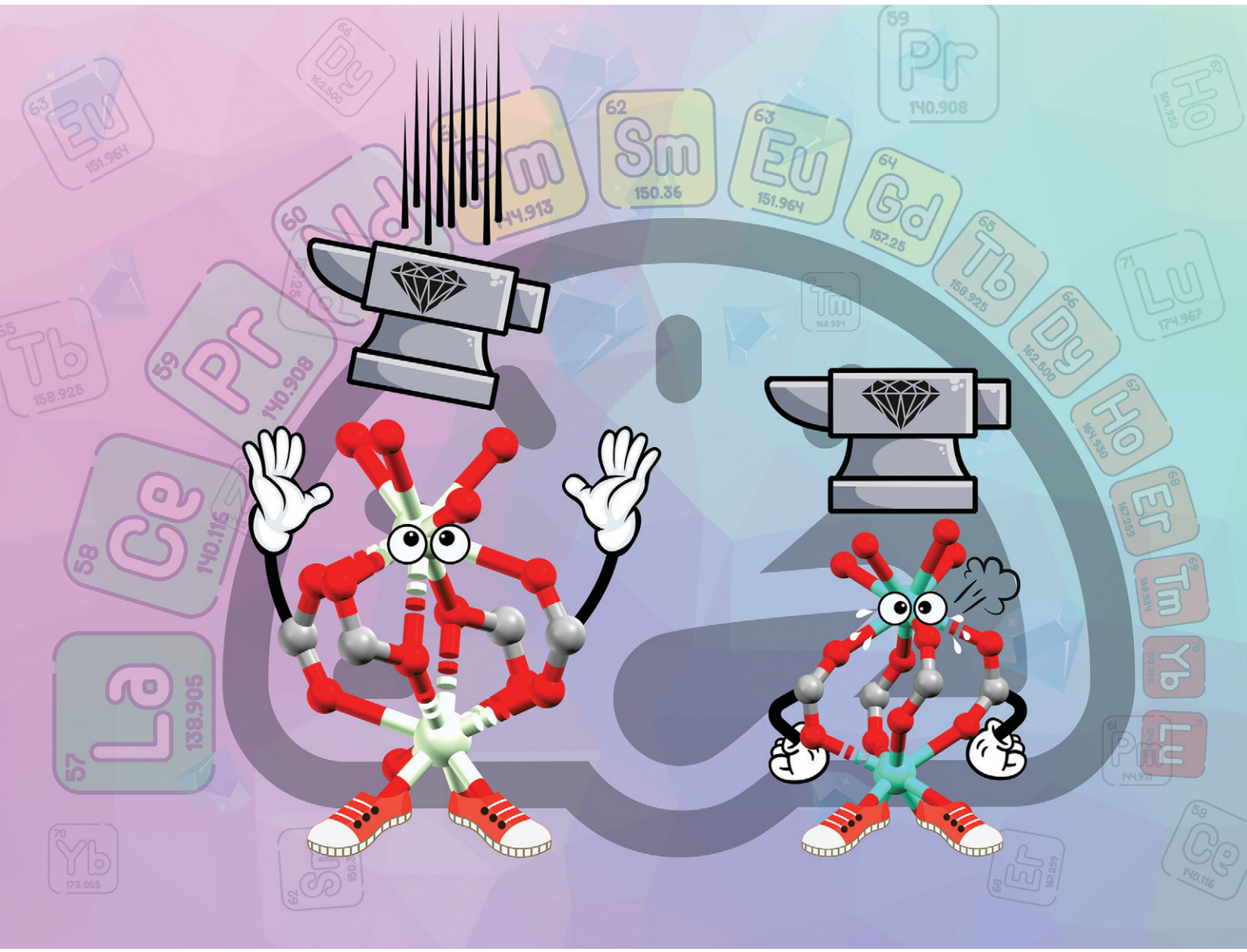

ISSN 1466-8033

ROYAL SOCIETY OF CHEMISTRY

COMMUNICATION

Lucy Hunter *et al.*

A reversible pressure-induced bond rearrangement of flexible lanthanide 2,5-bis(allyloxy)terephthalate coordination polymer networks

CrystEngComm

COMMUNICATION

View Article Online
View Journal | View Issue

Cite this: *CrystEngComm*, 2022, **24**, 8208

Received 8th April 2022,
Accepted 28th October 2022

DOI: 10.1039/d2ce00499b

rsc.li/crystengcomm

A reversible pressure-induced bond rearrangement of flexible lanthanide 2,5-bis(allyloxy)terephthalate coordination polymer networks†

L. R. Hunter, *[a] J. D. Sellars [bc] and M. R. Probert *[a]

Flexible coordination polymer networks reveal a plethora of structural transformations when exposed to high pressure as an external stimulus. Transformations are driven through organic linkers in a variety of ways, such as bond rotations, rearrangements and conformational shifts. We have successfully synthesised two sets of isostructural lanthanide coordination polymer networks that differ as a consequence of the lanthanide contraction. We have demonstrated that a pressure-induced reversible phase transition is possible between the two structurally distinct sets of networks. The system demonstrates a bond rearrangement due to an alteration of carboxylic acid binding modes from the 2,5-bis(allyloxy)terephthalate linker in addition to bond rotations within the flexible carbon backbone of the linker between 30–35 kbar.

1. Introduction

Coordination polymer networks (CPs) and metal–organic frameworks (MOFs) were originally sought for their structural stability and rigidity. However, more recently the focus has been to engineer dynamic 'sponge-like', porous, frameworks that offer greater opportunity for unique structural transformations. These dynamic frameworks allow transformations that lead to interesting and unique applications, such as enhanced proton conductivity,[1] plastically flexible crystals,[2] controlled drug delivery,[3] increased gas storage capabilities[4] and uses as mechanical shock absorbers.[5,6]

Several external stimuli, such as light,[7] heat[8] and pressure[9–12] can be utilised to create conditions to manipulate the dynamic nature of these frameworks. The study that first brought attention to flexible MOFs centred on MIL-53, a chromium-based MOF, termed the 'breathing framework'. Initially, it was recognised that MIL-53's diamond shaped pores could reversibly shrink by 5 Å in length in response to guest absorption and removal of H_2O.[13,14] Nevertheless, it was later realised that the use of pressure up to 10 kbar is another route to probe this transition.[15,16]

To explore potential structural transformations further, the incorporation of flexible organic linkers in CPs and MOFs allows a greater variety of physical responses to be investigated under extreme conditions. Networks can respond with familiar movements under high pressure conditions, including unit cell contractions,[17] bond orientation transformations, and negative linear compressibility.[18–20] More notable changes include solid state amorphisation,[21] phase transitions[22] and bond connectivity changes.[23] Nevertheless, a transformation involving bond connectivity transitions/rearrangements under extreme pressure conditions are rare, with reversibility of this even more scarce.[24] Herein, we report the synthesis of seven new lanthanide-based coordination polymer networks, that exhibit a distinct structural change in line with the lanthanide contraction (Fig. 1). The variation in global structure between sets is a repercussion of the decrease in coordination environment from 9 coordinate to 8 coordinate across the lanthanide series. Moreover, early lanthanide polymer networks undergo an interesting bond connectivity change at 30–35 kbar, whereby the carboxylic acid binding mode switches to that seen in lanthanide polymer networks later in the series, whilst retaining crystallinity, *i.e.* the pressure increase mimics the same structural change as the lanthanide contraction effect.

2. Crystal structure analysis

The lanthanide coordination polymer networks synthesised are all 2D non interpenetrating dense frameworks and all

[a] *Chemistry, School of Natural and Environmental Sciences, Newcastle University, Newcastle upon Tyne, NE1 7RU, UK. E-mail: l.hunter6@newcastle.ac.uk, michael.probert@newcastle.ac.uk*
[b] *Biosciences Institute, Faculty of Medical Sciences, Newcastle University, Newcastle upon Tyne NE2 4HH, UK*
[c] *School of Pharmacy, Faculty of Medical Sciences, King George VI Building, Newcastle upon Tyne NE1 7RU, UK*

† Electronic supplementary information (ESI) available. CCDC 2165369, 2165370, 2165373, 2165377, 2165388, 2165389, 2165394, 2165395, 2165397, 2165431, 2214554 and 2214557. For ESI and crystallographic data in CIF or other electronic format see DOI: https://doi.org/10.1039/d2ce00499b

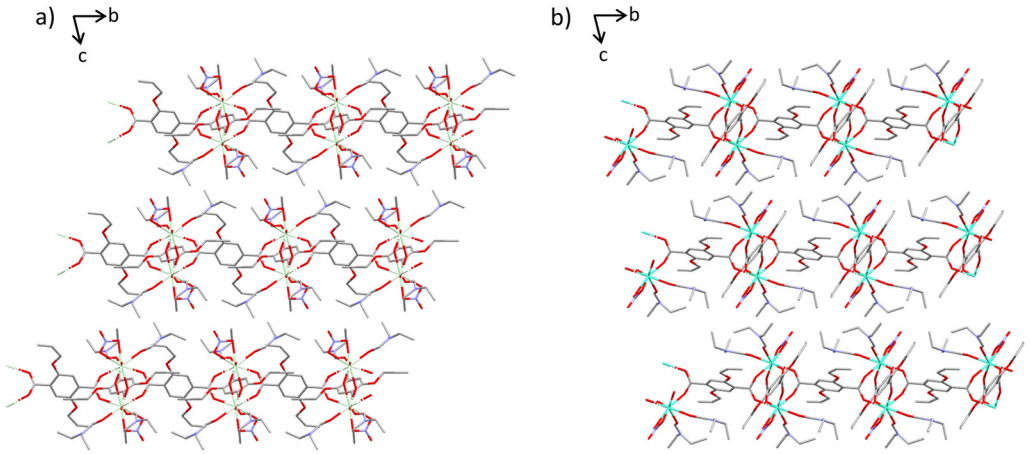

Fig. 1 a.) Complexes **1–3** viewed down the *a*-axis showing the 2D layered nature of the coordination polymers, linked by dimeric subunits; b.) Complexes **4–7** viewed down the *a*-axis. These representations show the similarities between the two sets of polymers in terms of both the local and global structure. Hydrogen atoms are omitted for clarity. Ln metal – cream/green, C – grey, O – red, N – blue.

frameworks crystallise in the $P\bar{1}$ space group. There are two subsets of network crystallised *via* the same conditions, this is hypothesised as a direct consequence of the lanthanide contraction (Fig. 1). Early metals in the series Ce–Nd, complexes **1–3**, possess a coordination number of nine, whereas metals later in the lanthanide series Eu–Dy, complexes **4–7**, have a coordination number of eight. This trend follows the decreasing ionic radius across the lanthanide series. Complexes **1–3** are isostructural, as are complexes **4–7**. All seven complexes consist of a dimeric subunit containing four linkers, two nitrate ions and four diethyl formamide solvent molecules. The difference in unit cell parameters, coordination number and consequently the secondary building unit structure between the two sets of networks arises from the bridging mode of the carboxylate-based linkers. Complexes **1–3** contain dimeric subunits with two distinct carboxylate binding modes. Two linkers bridge the metal centres *via* the commonly seen bidentate bridge μ_2–η^2, whilst the other two linkers bridge the metal centres *via* an μ_2–η^1, η^2 mode. In complexes **4–7** all four linkers bridge the two lanthanide metals only in an μ_2–η^2 mode. This gives rise to a distorted paddle wheel like geometry (Fig. 2c and d), commonly seen in Cu(II) MOF chemistry.[25]

Once grown, both sets of structures create a dense sheet that lies in the *ab* plane. There are no solvent accessible voids dispersed throughout the structures with all networks occupying approximately 65% of the unit cell volume. The largest spherical void radius within networks **1–3** is 1.2 Å, whereas for networks **4–7** it is 1.0 Å (Fig. S2†). One more notable difference between complexes **1–3** and **4–7** is the rotameric form of the extended allyloxy chains on the linkers. Complexes **1–3** have two separate orientations of carbon chain within the same polymer network. When viewing down the C–O bond that extends from the aromatic centroid, you can see the torsion angle of the chain sits in both an eclipsed and staggered positioning within the same polymer (Fig. 2b). The eclipsed torsion angle sits at 2.5°(9) and the staggered torsion angle sits at 130.2°(9). In complexes **4–7** only the eclipsed orientation of the linker exists.

3. High pressure experiments

To study the dynamic nature of the complexes **1–7**, high pressure studies were conducted, with a general procedure outlined below. A crystal was placed in a diamond anvil cell (DAC) containing a pentane/isopentane 1 : 1 mixture with diamond culets of 0.8 mm. The crystal occupies a sample chamber created by a stainless-steel gasket of 0.25 mm thickness, pre-indented to 0.15 mm with a precision drilled hole of 300 μm. A spherical ruby contained within the sample chamber facilitates pressure determination utilising fluorescence measurements.[26] To begin, the pressure was increased in 5 kbar increments until there was a notable change in unit cell parameters. The DAC was mounted directly onto the goniometer of XIPHOS II, a four circle Huber diffractometer with Ag–Kα IμS generator. High pressure data were collected and processed using the Bruker APEX software suites, which incorporates SAINT and SADABS for integration, cell refinement, and scaling.[27] The SHELX program suite was used for structure solution and refinement of all structures within the OLEX2 interface.[28] The data completeness of structures measured at high pressure is severely reduced due to the constraints placed on data collection when using a diamond anvil cell, for information see relevant CIF files.

A crystal of complex **2** was placed in the diamond anvil cell and was subjected to pressure increases of 5 kbar increments up to 35 kbar. Between 30 and 35 kbar a notable, first order, phase transition was observed (Fig. S1†). At this pressure, the unit cell axis lengths stay relatively constant whilst the angles show a significant shift compared to the ambient pressure structure. Parameters alter from α = 109.416(3)°, β = 95.138(3)°, γ = 95.947(3)°, to α = 98.203(4)°, β = 111.376(4)°, γ = 91.2570(2)° in addition to a considerable

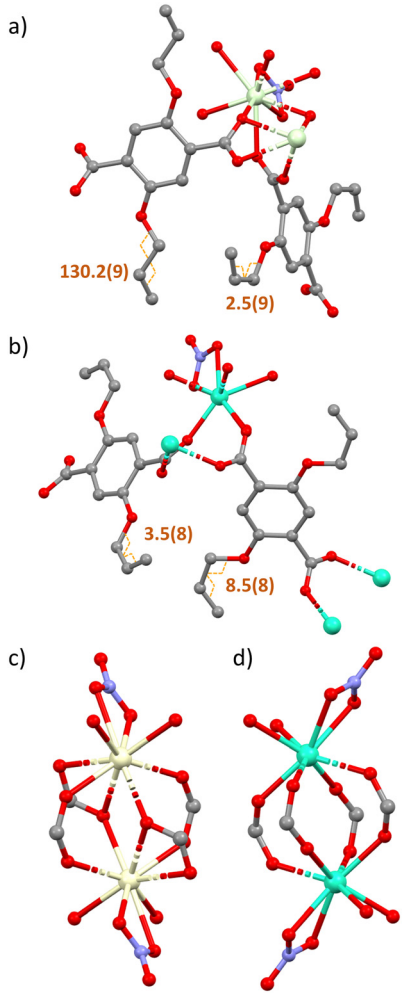

Fig. 2 A closer inspection of the molecular subunits and secondary building units of complexes **1**–**3** (a and c) and **4**–**7** (b and d). Complexes **1**–**3** incorporate eclipsed and staggered allyloxy groups, whereas complexes **4**–**7** contain only the eclipsed orientation. Orange labels in figures a) and b) denote the allyloxy torsion angles in degrees. Images c and d take a closer look at the secondary building units, clearly showing the different binding modes in each isostructural set. Hydrogen atoms are omitted for clarity. Ln metal – cream/green, C – grey, O – red, N – blue.

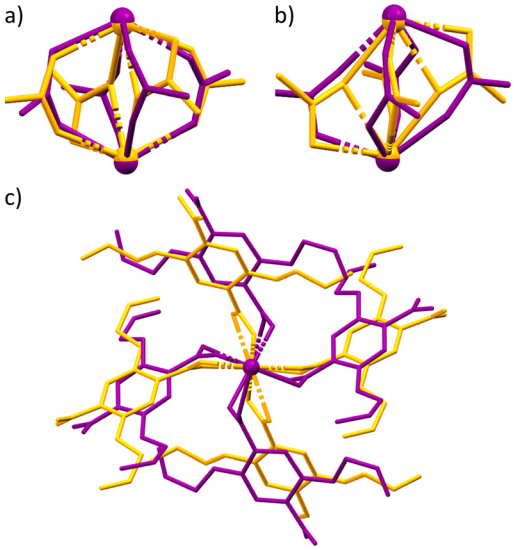

Fig. 3 Overlaid views of complex **2** at atmospheric pressure (orange) and at 35 kbar (purple). a) and b) Show two different orientations of the overlaid secondary building units, whereby you can visualise the change in carboxylic acid binding mode. c.) Shows a view along eclipsing metal centres, where you can see the anti-clockwise rotation of linkers under high pressure.

decrease in unit cell volume from 1420.2(2) $Å^3$ to 1208.43(11) $Å^3$. This displacement in cell parameters is accommodated in several ways. Most interestingly, the coordination number of the Praseodymium metal centre decreases by one as a Pr–O bond is broken. This is facilitated by the binding mode of two carboxylate ligands changing from μ_2–η^1, η^2 to μ_2–η^2 (Fig. 3a and b). Consequently, the secondary building unit (SBU) opens and the metal–metal distance increases from 4.112(4) Å to 4.329(2) Å. Alongside these significant structural changes, when the complex is viewed down the axis eclipsing the two metal centres a clockwise rotation is observed with the four linkers, that when combined with the increase in metal–metal centre distance imitates a corkscrew-like motion (Fig. 3c). Notwithstanding this, further adaptations can be observed, with the alkene 'arms' at atmospheric pressure occupying both an eclipsed and staggered geometry whilst at higher pressures they transform to an exclusively eclipsed orientation. All these structural transformations, once coupled together, convert the unit cell parameters of complex **2**, to mirror those observed in complexes **4**–**7**.

Whilst these changes are notable, we wanted to understand the potential reversibility of this process. To achieve this, the pressure within the diamond anvil cell was reduced in increments of 5 kbar. At 25 kbar the unit cell parameters were seen to rebound to near their former values of α = 109.464(3)°, β = 94.951(3)°, γ = 96.1010(3)° whilst the volume returned to 1458.24(11) $Å^3$. Upon return to atmospheric pressure and performing a full data collection, we see clearly the reversion of the SBU, with reinstatement of the coordination number of Pr back to nine and the binding mode of the two carboxylic acid linkers alters to μ_2–η^1, η^2 and the extra M–O bond is reformed, all whilst retaining crystallinity throughout these measurements. As a result, this system represents a fully reversible single crystal to single crystal transition when exposed to external pressure manipulation. Further images of this transformation can be visualised in Fig. S4 of the ESI.†

To understand how complexes **4**–**7** behaved under high pressure conditions, a crystal of complex **6** was placed in a diamond anvil cell using the same experimental methods. Pressure was applied to the DAC in 5 kbar increments up to 25 kbar. When applying a pressure of 5 kbar we see an initial compression of the unit cell, resulting in a volume decrease of ~185 $Å^3$ (Fig. S3†). The volume of the unit cell is now comparable to complex **2** at 35 kbar. When applying further pressure up to 25 kbar, unit cell parameters stay relatively constant within the margin of error reported, no significant

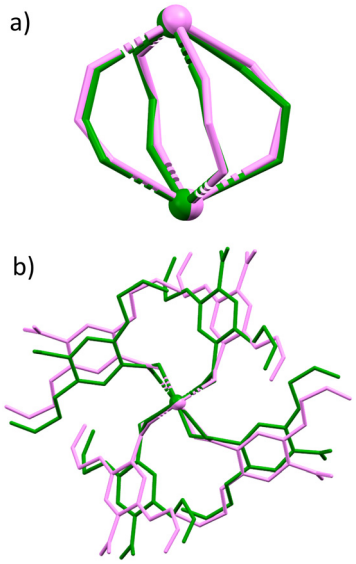

Fig. 4 Overlaid views of complex **6** at atmospheric pressure (green) and at 25 kbar (pink). a.) Shows the overlaid secondary building units. b.) Shows a view along eclipsing metal centres. The image shows the distortion of the network units, whereby you can observe the tilt angle changes for all four linkers.

transition was observed. By 25 kbar axis lengths decrease by less than 5.5% in all directions with compression at its largest along the *a*-axis from 10.4991(13) Å to 9.8113(6) Å. When overlaying the SBU's measured at atmospheric pressure and 25 kbar it is apparent that the changes observed are negligible with a minor displacement in the orientation of linkers in each of the dimeric subunits when viewing down the eclipsed metal centres (Fig. 4b).

Conclusion

We have successfully synthesized seven new coordination polymers using the 2,5-bis(allyloxy)terephthalate linker and lanthanide nitrate salts. These CPs can be separated into two sets of isostructural networks which are dependent upon the size of the metal ion incorporated. When placing the CP's containing larger lanthanide ions under pressures up to 35 kbar, the unit cell parameters alter to mimic the structures already synthesised using the smaller lanthanide ions. This change is facilitated in two ways. Firstly, a bond rearrangement from a μ_2–η^1, η^2 to a μ_2–η^2 carboxylic acid binding mode, and also bond rotations of the flexible 'arm' from a staggered to eclipsed torsion. The noted first order phase transition is reversible and networks can return to their former unit cell parameters at 25 kbar.

Associated content

Supporting information contains the synthetic route to 2,5-bis(allyloxy)terephthalate, IR, crystallographic information file data, void space plots, and high pressure data.

Conflicts of interest

There are no conflicts of interest.

Acknowledgements

The authors wish to thank Newcastle University's School of Natural and Environmental Sciences for funding this body of research.

Notes and references

1 D. Umeyama, S. Horike, C. Tassel, H. Kageyama, Y. Higo, K. Hagi, N. Ogiwara and S. Kitagawa, *APL Mater.*, 2014, **2**, 124401–124405.
2 X. Liu, A. A. L. Michalchuk, B. Bhattacharya, N. Yasuda, F. Emmerling and C. R. Pulham, *Nat. Commun.*, 2021, **12**, 1–8.
3 K. Jiang, L. Zhang, Q. Hu, D. Zhao, T. Xia, W. Lin, Y. Yang, Y. Cui, Y. Yang and G. Qian, *J. Mater. Chem. B*, 2016, **4**, 6398–6401.
4 H. Li, L. Li, R.-B. Lin, W. Zhou, Z. Zhang, S. Xiang and B. Chen, *EnergyChem*, 2019, **1**, 100006–100045.
5 P. G. Yot, Z. Boudene, J. Macia, D. Granier, L. Vanduyfhuys, T. Verstraelen, V. Van Speybroeck, T. Devic, C. Serre, G. Férey, N. Stock and G. Maurin, *Chem. Commun.*, 2014, **50**, 9462–9464.
6 X. Zhou, Y. Miao, K. S. Suslick and D. D. Dlott, *Acc. Chem. Res.*, 2020, **53**, 2806–2815.
7 I. M. Walton, J. M. Cox, C. A. Benson, D. G. Patel, Y. S. Chen and J. B. Benedict, *New J. Chem.*, 2016, **40**, 101–106.
8 A. Karmakar, P. G. M. Mileo, I. Bok, S. B. Peh, J. Zhang, H. Yuan, G. Maurin and D. Zhao, *Angew. Chem., Int. Ed.*, 2020, **132**, 11096–11102.
9 L. Bolinois, T. Kundu, X. Wang, Y. Wang, Z. Hu, K. Koh and D. Zhao, *Chem. Commun.*, 2017, **53**, 8118–8121.
10 I. E. Collings and A. L. Goodwin, *J. Appl. Phys.*, 2019, **126**, 181101–181113.
11 P. Zhao, T. D. Bennett, N. P. M. Casati, G. I. Lampronti, S. A. Moggach and S. A. T. Redfern, *Dalton Trans.*, 2015, **44**, 4498–4503.
12 W. Cai, A. Gładysiak, M. Anioła, V. J. Smith, L. J. Barbour and A. Katrusiak, *J. Am. Chem. Soc.*, 2015, **137**, 9296–9301.
13 C. Serre, F. Millange, C. Thouvenot, M. Noguès, G. Marsolier, D. Louër and G. Férey, *J. Am. Chem. Soc.*, 2002, **124**, 13519–13526.
14 A. V. Neimark, F. X. Coudert, C. Triguero, A. Boutin, A. H. Fuchs, I. Beurroies and R. Denoyel, *Langmuir*, 2011, **27**, 4734–4741.
15 (*a*) L. B. I. Beurroies, M. Boulhout, P. L. Llewellyn, B. Kuchta, G. Férey, C. Serre and R. Denoyel, *Angew. Chem., Int. Ed.*, 2010, **49**, 7526–7529; (*b*) P. Serra-Crespo, A. Dikhtiarenko, E. Stavitski, J. Juan-Alcañiz, F. Kapteijn, F. X. Coudert and J. Gascon, *CrystEngComm*, 2015, **17**, 276–280.
16 M. Wahiduzzaman, N. Reimer, J. P. Itié, N. Stock, G. Maurin and P. G. Yot, *Polyhedron*, 2018, **155**, 144–148.
17 P. G. Yot, Q. Ma, J. Haines, Q. Yang, A. Ghoufi, T. Devic, C. Serre, V. Dmitriev, G. Férey, C. Zhong and G. Maurin, *Chem. Sci.*, 2012, **3**, 1100.

18 A. Sussardi, C. L. Hobday, R. J. Marshall, R. S. Forgan, A. C. Jones and S. A. Moggach, *Angew. Chem., Int. Ed.*, 2020, **59**, 8118–8122.
19 W. Li, M. R. Probert, M. Kosa, T. D. Bennett, A. Thirumurugan, R. P. Burwood, M. Parinello, J. A. K. Howard and A. K. Cheetham, *J. Am. Chem. Soc.*, 2012, **134**, 11940–11943.
20 A. B. Cairns, J. Catafesta, C. Levelut, J. Rouquette, A. Van Der Lee, L. Peters, A. L. Thompson, V. Dmitriev, J. Haines and A. L. Goodwin, *Nat. Mater.*, 2013, **12**, 212–216.
21 K. W. Chapman, D. F. Sava, G. J. Halder, P. J. Chupas and T. M. Nenoff, *J. Am. Chem. Soc.*, 2011, **133**, 18583–18585.
22 M. Zhou, K. Wang, Z. Men, C. Sun, Z. Li, B. Liu, G. Zou and B. Zou, *CrystEngComm*, 2014, **16**, 4084–4087.
23 J. K. Clegg, A. J. Brock, K. A. Jolliffe, L. F. Lindoy, S. Parsons, P. A. Tasker and F. J. White, *Chem. – Eur. J.*, 2017, **23**, 12480–12483.
24 E. C. Spencer, M. S. R. N. Kiran, W. Li, U. Ramamurty, N. L. Ross and A. K. Cheetham, *Angew. Chem., Int. Ed.*, 2014, **53**, 5583–5586.
25 Y. Chen, B. Wang, X. Wang, L. H. Xie, J. Li, Y. Xie and J. R. Li, *ACS Appl. Mater. Interfaces*, 2017, **9**, 27027–27035.
26 G. J. Piermarini, S. Block, J. D. Barnett and R. A. Forman, *J. Appl. Phys.*, 1975, **46**, 2774–2780.
27 T. Schulz, K. Meindl, D. Leusser, D. Stern, J. Graf, C. Michaelsen, M. Ruf, G. M. Sheldrick and D. Stalke, *J. Appl. Crystallogr.*, 2009, **42**, 885–891.
28 G. M. Sheldrick, *Acta Crystallogr., Sect. A: Found. Crystallogr.*, 2008, **64**, 112.

